Proceedings of the 20th International Conference on Soil Mechanics and Geotechnical Engineering– Rahman and Jaksa (Eds)

A vector-IM based fragility model for man-made earth slopes subject to seismic shaking

Un modèle de fragilité basé sur l'IM vectorielle pour les pentes de terre artificielles sujettes à des secousses sismiques

Wenqi Du, Wei Wang & Dian-Qing Li

State Key Laboratory of Water Resources and Hydropower Engineering Science, Institute of Engineering Risk and Disaster Prevention, Wuhan University, China, wqdu309@whu.edu.cn

ABSTRACT: Seismic fragility analysis is an important topic in earthquake engineering field. A scalar intensity measure (IM) is commonly used for describing the seismic fragility relationships, whereas fragility models using a vector-IM as indicators are relatively limited. In this study, a vector-IM based fragility model is presented for assessing the seismic vulnerability of man-made earth slopes. A set of 332 ground motions are first selected covering a wide range of moment magnitudes and source-to-site distances. Non-linear dynamic analyses are then conducted for a generic earth slope implemented in FLAC; several fragility models are developed based on the cloud analysis. Subsequently, the efficiency and sufficiency of several commonly used scalar and vector IMs are compared, determining the most appropriate vector-IM as indicators for seismic fragility analysis. The results demonstrate that the appropriate scalar and vector IMs for conducting the fragility analysis of earth slopes are Sa(Ts), PGA, ASI, and [Sa(Ts), Ia], respectively. The vector-IM based fragility model developed can be used for assessing the seismic damage of earth slopes in engineering applications.

RÉSUMÉ : L'analyse de la fragilité sismique est un sujet important dans le domaine de l'ingénierie sismique. Une mesure d'intensité scalaire (IM) est couramment utilisée pour décrire les relations de fragilité sismique, alors que les modèles de fragilité utilisant un vecteur-IM comme indicateurs sont relativement limités. Dans cette étude, un modèle de fragilité basé sur la MN vectorielle est présenté pour évaluer la vulnérabilité sismique des pentes de terre artificielles. Un ensemble de 332 mouvements du sol est d'abord sélectionné couvrant une large gamme de magnitudes de moment et de distances source-site. Des analyses dynamiques non linéaires sont ensuite effectuées pour une pente de terre générique implémentée dans FLAC; plusieurs modèles de fragilité sont développés à partir de l'analyse du cloud. Par la suite, l'efficacité et la suffisance de plusieurs IM scalaires et vectorielles couramment utilisées sont comparées, déterminant la IM vectorielle la plus appropriée comme indicateurs pour l'analyse de fragilité sismique. Les résultats démontrent que les IM scalaires et vectorielles appropriées pour mener l'analyse de fragilité des pentes de la terre sont respectivement Sa(Ts), PGA, ASI et [Sa(Ts), Ia]. Le modèle de fragilité basé sur l'IM vectorielle développé peut être utilisé pour évaluer les dommages sismiques des pentes terrestres dans les applications d'ingénierie.

KEYWORDS: earth slope; fragility analysis; intensity measures; cloud analysis; limit state

1 INTRODUCTION

Man-made earth slopes, such as embankments and cuts, are widely distributed in highway and railway networks. During past major earthquakes, different degrees of damage or even failure of earth slopes were frequently observed, resulting in huge losses of life and property (Maruyama et al. 2010, Argyroudis et al. 2019). Therefore, it is important to conduct the seismic risk analysis of earth slopes in engineering practice.

Seismic fragility analysis is one of the key components in the probabilistic seismic risk assessment. A fragility function (i.e., fragility model) describes a structure's probability of exceeding some limit states, expressed as a function of a given ground motion intensity measure (IM) (Baker 2015). The limit state (LS) is commonly defined in terms of engineering demand parameters (EDPs), including the maximum inter-story drift ratio for reinforced concrete buildings (Du et al. 2020), tilting for caisson quay walls (Jafarian & Miraei 2019), and relative settlement rate for earth-rockfill dams (Jin & Chi 2019). As for slope systems, many researches (Lagaros 2009, Wu 2015, Huang et al. 2018, Hu et al. 2019) have taken the factor of safety as EDP. Besides, Argyroudis and Kaynia (2015) adopted the permanent settlement, and proposed a set of fragility curves for embankments and cuts with various features.

The selection of IM plays an important role in developing the fragility function, since the results based on various IMs could be significantly different (Jafarian & Miraei 2019). The selection of an appropriate IM in earthquake engineering is usually guided by the 'efficiency' and 'sufficiency' criteria, as introduced by Shome(1999), Luco (2002), and Jalayer (2003). Since then, some researches (Luco & Cornell 2007, Padgett et al. 2008, Hariri-Ardebili & Saouma 2016) have also proposed additional criteria for selecting appropriate IMs, such as practicality, proficiency, and hazard compatibility. Furthermore, many researchers (e.g., Baker & Cornell 2008, Wang & Du 2012) have stated that, a single IM (i.e., scalar-IM) cannot represent the intrinsic complex characteristics of seismic shaking. Therefore, many efforts have been made to employing multiple IMs (i.e., vector-IM) for conducting seismic risk evaluations (Baker 2005, Pan et al. 2010, Jalayer et al. 2012, Gehl et al. 2013, Du & Wang 2014, Yakhchalian et al. 2015). Due to the additional information provided by a secondary IM, the use of a vector-IM is, to some extent, advantageous over the scalar-IM.

The aim of this paper is to identify the appropriate scalar- and vector-IM for conducting the fragility analysis of slopes, and thus propose a vector-IM based fragility model for man-made earth slopes. The remaining part of this paper is organized as follows. The IMs considered in this study are introduced in Section 2. A numerical man-made slope model is presented in Section 3. The process of selecting optimal IMs and developing vector-IM based fragility model is described in detail in Section 4. Finally, discussions and conclusions are given in Section 5.

2 IMS CONSIDERED

In existing literatures, many IMs have been proposed to characterize the characteristics of ground motions, such as the amplitude, frequency content, and duration. In this study, nine

commonly used IMs are regarded as candidate predictor variables in developing fragility models.

The amplitude-related parameters, namely peak ground acceleration (PGA) and peak ground velocity (PGV), are the most widely used IMs in earthquake engineering practice. These two parameters are defined as:

$$\mathrm{PGA} = \max\left(\left|a(t)\right|\right) \tag{1}$$

$$\mathrm{PGV} = \max\left(\left|v(t)\right|\right) \tag{2}$$

where $a(t)$ and $v(t)$ denote the acceleration- and velocity-time histories of a ground-motion record, respectively.

Cumulative absolute velocity (CAV) is defined as the integral of the absolute value of the acceleration-time history (EPRI-NP-5930 1988):

$$\mathrm{CAV} = \int_0^{T_r} \left|a(t)\right| \mathrm{d}t \tag{3}$$

where T_r is the total time of a record.

Arias intensity (Ia), as defined by Arias (1970), is a measure of the total energy content of a ground motion:

$$\mathrm{Ia} = \frac{\pi}{2g} \int_0^{T_r} a^2(t) \mathrm{d}t \tag{4}$$

in which g denotes the acceleration of gravity.

Spectral acceleration at the fundamental period (Ts) of a structure, Sa(Ts), is another widely used IM in earthquake engineering. In addition, previous studies have shown that the spectral acceleration at a degraded period of 1.5Ts, Sa(1.5Ts), is appropriate to estimate the earthquake-induced slope displacement (Bray & Travosora 2007, Du et al. 2018). Unline the two spectral IMs as stated above, the next two IMs, namely acceleration spectrum intensity (ASI) and velocity spectrum intensity (VSI), are structure independent, representing the severity of the short period content of a ground motion (Von et al. 1988, Bradley 2011):

$$\mathrm{ASI} = \int_{0.1}^{0.5} Sa(T, \xi = 5\%) \mathrm{d}T \tag{5}$$

$$\mathrm{VSI} = \int_{0.1}^{2.5} Sv(T, \xi = 5\%) \mathrm{d}T \tag{6}$$

where Sa and Sv are the acceleration and velocity response spectrum, respectively; T dentoes the vibration period; and ξ is the damping ratio.

Finally, the duration-related parameter, significant duration $\mathrm{Ds}_{5\text{-}75}$, is defined as the time interval over which 5-75% of Ia is accumulated (Trifunac & Brady 1975). It is worth noting that all the IMs considered herein, associated with their descriptions and units, are summarized in Table 1.

Table 1. Nine intensity measures considered in this study

Intensity measure	Description	Units
PGA	Peak ground acceleration	g
PGV	Peak ground velocity	cm/s
CAV	Cumulative absolute velocity	m/s
Ia	Arias intensity	m/s
Sa(Ts)	Spectral acceleration at Ts	g
Sa(1.5Ts)	Spectral acceleration at 1.5Ts	g
ASI	Acceleration spectrum intensity	g*s
VSI	Velocity spectrum intensity	m
$\mathrm{Ds}_{5\text{-}75}$	Significant duration	s

3 NUMERICAL SLOPE MODEL

3.1 *Overview*

A generic earth slope model and subsequent non-linear dynamic analyses for this slope are conducted in *FLAC* (Itasca Consulting Group Inc. 2016). The two-dimensional slope model is schematically illustrated in Fig. 1. Its height and inclination are 8 m and 45° (i.e., slope gradient 1:1), respectively. The strata of this slope-foundation system from top to bottom are a 4-m-thick clay layer, a 4-m-thick silty clay layer, a 10-m-thick silty sand layer, and a 10-m-thick bedrock layer, respectively. The density, strength, and stiffness parameters of each stratum are tabulated in Table 2. The estimated Ts of this slope is 0.20 s based on a free-vibration analysis.

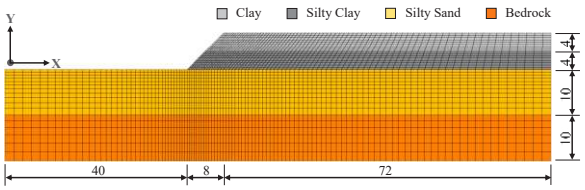

Figure 1. Schematic representation of a man-made earth slope (unit: m).

3.2 *Constitutive model and soil modules degradation*

The dynamic response of the slope is controlled by a modified constitutive model, which has been implemented in *FLAC* (Itasca Consulting Group Inc. 2016, Wang et al. 2021). The modified constitutive model combines the hysteretic damping formulation with the well-known Mohr-Coulomb strength criterion, which is capable of quantifying the cyclic dissipation during the elastic phase and reproducing the irreversible strain accumulation that may occur during seismic shaking. In the elastic stage, the tangent shear modulus is adjusted to match an empirical modulus reduction curve proposed by Hardin and Drnevich (1972a, 1972b):

$$M_S = \frac{G}{G_0} = \frac{1}{1 + \gamma/\gamma_{\mathrm{ref}}}, \ \gamma \le \gamma_{\mathrm{m}} \tag{7}$$

where M_S is the shear modulus reduction factor; γ denotes shear strain; γ_{m} denotes the yield shear strain; and γ_{ref} is the reference strain at which the modulus reduction curve crosses the $M_S = 0.5$ line. In the plastic stage, the shear modulus yields the following equation according to the ideal plasticity hypothesis:

$$M_S = \frac{1}{\left(1 + \gamma_{\mathrm{m}}/\gamma_{\mathrm{ref}}\right)\gamma/\gamma_{\mathrm{m}}}, \ \gamma > \gamma_{\mathrm{m}} \tag{8}$$

Besides the hysteretic damping, we also assign a 0.2% stiffness-proportional component of Rayleigh damping in order to remove the high frequency noise.

Table 2. Parameters assigned to each slope-foundation layer.

Stratum	Density ρ (kg·m^{-3})	Cohesion c (kPa)	Friction φ (°)	Bulk modulus K_0 (MPa)	Shear modulus G_0 (MPa)	P-wave velocity C_{P0} (m·s^{-1})	S-wave velocity C_{S0} (m·s^{-1})	Reference strain γ_{ref} (%)
Clay	1,800	25	16	500	100	593	236	0.234
Silty clay	2,000	18	23	280	130	476	255	0.234
Silty sand	2,050	5	36	500	235	630	339	0.234
Bedrock	2,500	15,000	45	10,000	6,000	2,863	1,549	-

3.3 *Mesh size and boundary conditions*

The mesh size needs to be determined before conducting the dynamic analysis. As suggested in *FLAC*, the mesh size should not be larger than 1/8 of the wavelength corresponding to the highest frequency component of the input waves. The adopted mesh size therefore varies from 0.5 m to 2.0 m, as illustrated in Fig. 1.

The numerical simulation process is divided into two phases, namely the static phase and the dynamic phase. In the first phase, the horizontal movement of both lateral sides is fixed, and the movement of the bottom boundary is completely frozen. In the second phase, the free-field boundary is applied to both lateral sides, and the input motions are excited at the bottom of the numerical model.

4 CLOUD-BASED FRAGILITY ANALYSIS

4.1 *Brief introduction of the cloud analysis*

Cloud analysis (CLA) is one of the commonly used procedures to perform non-linear dynamic analysis (Jalayer 2003). Within the cloud analysis, all ground-motion records are used without any prior scaling, and a linear regression model needs to be established in logarithmic scale between EDP and IM (e.g., PGA). As summarized by Jalayer et al. (2017), there are three assumptions in developing the cloud-based regression model: (1) the EDP given IM follows a lognormal distribution; (2) a linear relationship exists between the mean EDP and logarithmic IM [Eq. (9)]; (3) the standard deviation of the model error (i.e., dispersion) remains constant for the whole IM range [Eq. (10)]. The relationshps are expressed as:

$$\ln \mu_{\mathrm{EDP}|\mathbf{IM}} = \ln a + \mathbf{b} \ln \mathbf{IM} \tag{9}$$

$$\beta_{\mathrm{EDP}|\mathbf{IM}} = \sqrt{\frac{\sum_{i=1}^{N} \left(\ln EDP_i - \ln \mu_{\mathrm{EDP}|\mathbf{IM},i} \right)^2}{N - N_{reg}}} \tag{10}$$

where $\mathbf{IM}$ denotes the vector-form IM; $\ln a$ and $\mathbf{b}$ are the regression parameters, and the length of $\mathbf{b}$ is determined by the length of $\mathbf{IM}$; N and N_{reg} are the numbers of records and the parameters employed in Eq. (9), respectively; $\mu_{\mathrm{EDP}|\mathbf{IM}}$ and $\beta_{\mathrm{EDP}|\mathbf{IM}}$ denote the mean and dispersion of an EDP given $\mathbf{IM}$, respectively.

It should be noting that, given some input motions having high shaking intensity, excessively large deformation beyond the validity of the constitutive model might be obtained, or even numerical non-convergence would happen in the dynamic process. These cases were referred to as 'collapse cases' for reinforced concrete structures in literatures (Jalayer & Cornell 2009). In this paper, these cases are similarly referred to as 'failure cases' for earth slopes. As a result, the dynamic results obtained can be divided into two parts: the failure data and un-failure data. The probability of failure can therefore be predicted by a logistic regression model (Jalayer et al. 2017):

$$P(F|\mathbf{IM}) = \frac{1}{1 + \mathrm{e}^{-(\theta_0 + \boldsymbol{\theta} \ln \mathbf{IM})}} \tag{11}$$

where θ_0 and $\boldsymbol{\theta}$ are the parameters of the logistic model, and the length of $\boldsymbol{\theta}$ is equal to that of $\mathbf{IM}$.

Consequently, based on the total probability theorem (Shome 1999, Jalayer et al. 2017), the fragility function incorporating the 'failure cases' can be derived as:

$$P(EDP > LS_i|\mathbf{IM}) = \Phi\left(\frac{\ln \mu_{\mathrm{EDP}|\mathbf{IM}} - \ln LS_i}{\beta_{\mathrm{EDP}|\mathbf{IM}}} \right) \cdot (1 - P(F|\mathbf{IM})) + P(F|\mathbf{IM}) \tag{12}$$

where $P(EDP > LS_i|\mathbf{IM})$ denotes the probability of exceeding the i-th limit state with the given $\mathbf{IM}$.

For the scalar-IM based fragility analysis, a 5-parameter fragility model can be obtained, with parameters denoted as $\mathbf{X}=[\ln a, b_1, \beta_{\mathrm{EDP}|\mathbf{IM}}, \theta_0, \theta_1]$ (Jalayer et al. 2017). Accordingly, the vector-IM based fragility analysis [i.e., $\mathbf{IM}=(IM_1, IM_2)$] can also be conducted, by developing a 7-parameter fragility model with $\mathbf{X}=[\ln a, b_1, b_2, \beta_{\mathrm{EDP}|\mathbf{IM}}, \theta_0, \theta_1, \theta_2]$.

4.2 *Ground motions selected*

A set of 332 ground-motion records are selected from the PEER NGA-West2 database (Ancheta, 2014). These records cover a wide range of moment magnitudes (M_w) between 5.5 and 7.5 and closest source-to-site distances (R_{rup}) up to 100 km. The moment magnitude versus distance distribution of the selected records is shown in Fig. 2a. The response spectra are illustrated in Fig. 2b. It is clear that the selected records cover a wide range of spectral acceleration ordinates. It is noted that all ground motions selected have Vs_{30} (average shear wave velocity in upper 30 meters) larger than 500 m/s.

4.3 *Definition of limit states*

In the seismic risk assessment, the limit states are defined as the thresholds between various damage categories, usually referred to as damage states. Different definitions of damage states have been proposed for various systems, such as HAZUS-MH for lifeline elements and transportation infrastructures (HAZUS-MH 2004), REDARS for highway systems (Werner et al. 2006), and PIANC for port structures (PIANC 2001). However, the definition of damage states for slope systems is relatively limited. To the authors' knowledge, only the European project SYNER-G defined the damage states for highway embankment and cut (Pitilakis et al. 2014). In this project, the permanent settlement at slope crest (YDisp) is considered as EDP, and three levels of

damage states are determined by this EDP accordingly (Pitilakis et al. 2014). Thus, following the classifications of SYNER-G, the damage states herein are defined as: stable (0-5 cm), minor damage (5-15 cm), moderate damage (15-40 cm) and complete failure (beyond 40 cm). Accordingly, the limit states are considered as follows: LS_1=5 cm, LS_2=15 cm, and LS_3=40 cm.

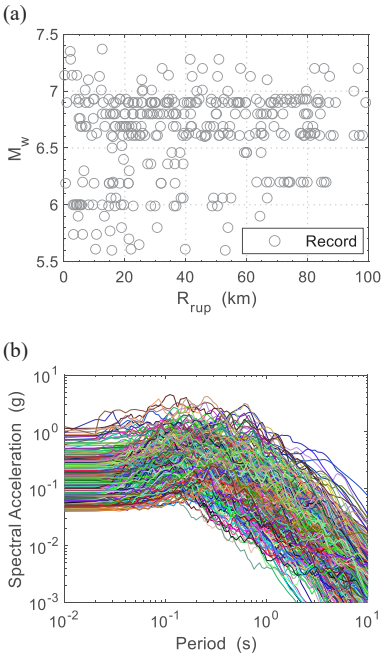

Figure 2. (a) M_w-R_{rup} distribution and (b) spectral shape for the selected records.

4.4 *Scalar-IM based fragility analysis*

Appropriate scalar- and vector-IMs needs to be selected before constructing a fragility model. In this study, the criteria of selecting appropriate IMs are based on the goodness-of-fit, efficiency, and sufficiency. A larger coefficient of determination (R^2) denotes higher correlation between EDP and IM. An efficient IM is capable of predicting EDP with relatively small variability. A sufficient IM, on the other hand, ensures the residuals of EDP given this IM being independent of moment magnitude and closest source-to-site distance (Luco & Cornell 2007). The dispersion ($\beta_{EDP|IM}$) is used to gauge the efficiency, and a lower $\beta_{EDP|IM}$ indicates a more efficient IM (Hariri-Ardebili & Saouma 2016). The slopes of the fitted lines of the residuals [$\log(\varepsilon|IM)$] with respect to M_w and R_{rup} (termed as S_M and S_R hereafter) are employed to gauge the sufficiency, and a smaller value of S_M or S_R indicates a more sufficient IM (Jafarian & Miraei 2019).

Linear regression models for the nine candidate scalar-IMs are illustrate in Fig. 3. As shown in this figure, four IMs including Sa(Ts), ASI, Ia, and PGA reveal modelate to strong correlation to the crest settlement ($R^2 > 0.7$), especially for Sa(Ts). The remaining IMs, namely Sa(1.5Ts), CAV, PGV, VSI and $Ds_{5\text{-}75}$, are weakly correlated to the settlement. Therefore, It seems not appropriate to choose the latter five IMs as predictor variables for developing a fragility function.

The efficiency and sufficiency of these scalar IMs are subsequently assessed, as summarized in Table 3. As expected, Sa(Ts), ASI, Ia, and PGA have relatively small values of $\beta_{EDP|IM}$, in which Sa(Ts) can be regarded as the most efficient scalar-IM. As for sufficiency, Fig. 4 illusrates the dependences of model resdiduals on M_w and R_{rup}, respectively. It is shown that, the IMs of ASI, PGA, and VSI do not exhibit a clear dependence on M_w, and Sa(Ts), ASI, and PGA do not exhibit a dependence on R_{rup}. It is thus indicated that only ASI and PGA satisfy the sufficiency criterion.

By constituting a reasonable trade-off between efficiency and sufficiency, the three IMs, namely Sa(Ts), ASI, and PGA could be considered as the appropriate IMs for conducting the scalar-IM based fragility analysis of man-made earth slopes. Fig. 5 demonstrates the fragility curves developed based on Sa(Ts).

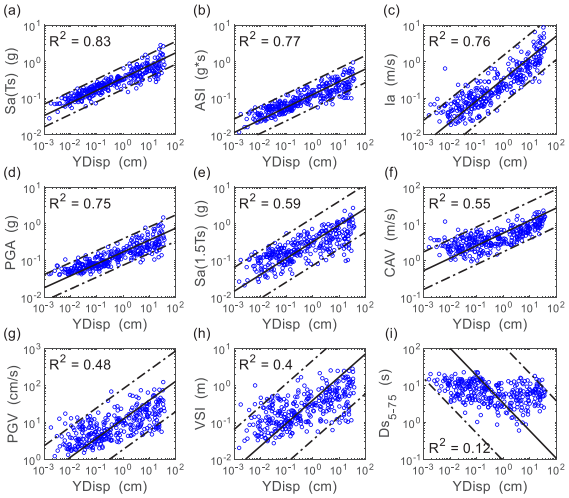

Figure 3. Linear regression models for the nine candidate scalar-IMs. The blue dots denote empirical data. The solid lines show the mean EDP given IM, and the dash dotted lines show the 95% confidence interval.

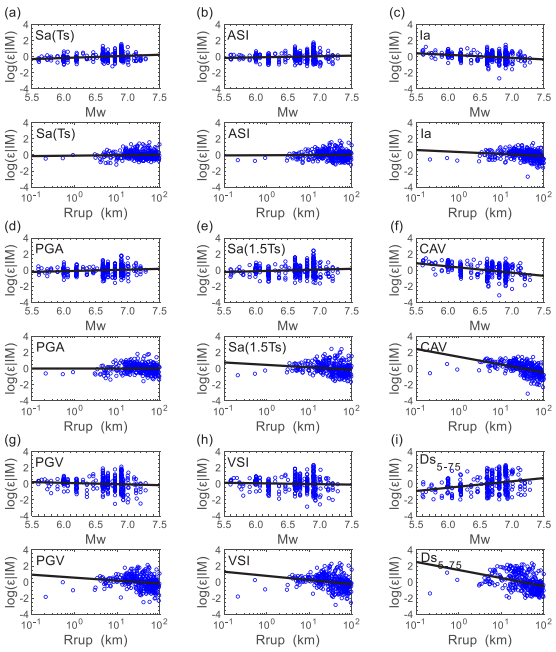

Figure 4. Dependences of model residuals on M_w and R_{rup} for these scalar IMs. The blue dots denote empirical data, and the lines show the fitted line of residuals with respect to moment magnitude and closest source-to-site distance, respectively.

4.5 *Vector-IM based fragility analysis*

As summarized in Table 4, a total of 21 vector-IMs composed of different combinations of two scalar IMs are examined. Compared with Table 3, it is clear that the goodness-of-fit, efficiency, and sufficiency are improved significantly by incorporating the additional IM. With more information provided by vector-IMs, an improved prediction of the damage probability of slopes could be obtained by using the vector-IM based fragility model. The process of selecting the optimal vector-IM is just

same as the scalar one. From Table 4, the vector-IM of [Sa(Ts), Ia] exhibits the best performance in terms of R^2, $\beta_{EDP|IM}$, and $S_M(S_R)$. Consequently, it is chosen as the optimal vector-IM. Fragility surfaces for man-made earth slope based on [Sa(Ts), Ia] are shown in Fig. 6. The parameters of the vector-IM based fragility model are **X**=[1.25, 1.94, 0.73, 0.39, -5.53, 8.73, 10.21].

Table 3. Comparison of goodness-of-fit, efficiency, and sufficiency for these scalar-IMs

IM	Sa(Ts)	ASI	Ia	PGA	Sa(1.5Ts)	CAV	PGV	VSI	$Ds_{5\text{-}75}$
R^2	0.83	0.77	0.76	0.75	0.59	0.55	0.48	0.40	0.12
$\beta_{EDP\|IM}$	0.46	0.54	0.56	0.57	0.73	0.77	0.82	0.88	1.07
S_M	0.27	0.14	-0.38	0.19	0.20	-0.78	-0.19	-0.11	0.80
S_R	0.06	0.02	-0.25	0.00	-0.30	-0.97	-0.37	-0.52	-1.00

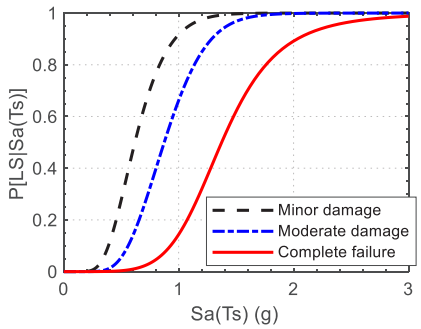

Figure 5. The fragility curves for man-made earth slope based on Sa(Ts).

Table 4. Comparison of the goodness-of-fit, efficiency, and sufficiency for vector-IMs

IM_1, IM_2	R^2	$\beta_{EDP\|IM}$	S_M	S_R
PGA, PGV	0.75	0.57	0.18	0.01
PGA, CAV	0.77	0.54	-0.10	-0.12
PGA, I_a	0.78	0.53	-0.12	-0.08
PGA, SED	0.75	0.56	0.12	0.01
PGA, Sa(Ts)	0.85	0.44	0.24	0.13
PGA, Sa(1.5Ts)	0.77	0.55	0.19	0.05
PGA, ASI	0.80	0.51	0.16	0.08
PGA, VSI	0.75	0.57	0.17	0.02
Sa(Ts), PGV	0.83	0.46	0.25	0.06
Sa(Ts), CAV	0.89	0.39	-0.14	-0.03
Sa(Ts), I_a	0.88	0.39	-0.01	0.08
Sa(Ts), SED	0.84	0.46	0.20	0.07
Sa(Ts), Sa(1.5Ts)	0.83	0.46	0.27	0.05
Sa(Ts), ASI	0.84	0.46	0.24	0.08
Sa(Ts), VSI	0.83	0.46	0.28	0.05
ASI, PGV	0.80	0.51	0.33	-0.02
ASI, CAV	0.82	0.49	-0.24	-0.09
ASI, I_a	0.82	0.48	-0.13	0.00
ASI, SED	0.78	0.53	0.31	0.02
ASI, Sa(1.5Ts)	0.81	0.49	0.11	0.06
ASI, VSI	0.81	0.50	0.31	-0.03

5 DISCUSSIONS AND CONCLUSIONS

A vector-IM based seismic fragility model for man-made earth slopes was proposed in this study. Non-linear dynamic analyses for a generic slope model were conducted in FLAC using 332 ground motions selected from the PEER NGA-West2 database. Permanent settlement at the slope crest was taken as the engineering demand parameter, which was also used to define the limit states. Several commonly used IMs were employed for identifying the appropriate IMs. Based on the cloud analysis, the scalar-IM and vector-IM based fragility analyses were conducted, respectively.

The appropriate scalar IMs for man-made earth slopes are Sa(Ts), PGA, and ASI, although the last one is seldom taken as the parameter for conducting fragility analysis. Besides, it is observed that the goodness-of-fit, efficiency, and sufficiency are improved significantly by using the vector-IMs, given the more complete information provided by the additional IMs. It is found that the optimal vector-IM for man-made earth slopes is [Sa(Ts), Ia]. The parameters of fragility model based on Sa(Ts) and [Sa(Ts), Ia] are **X**=[1.30, 2.92, 0.46, -1.79, 12.94] and **X**=[1.25, 1.94, 0.73, 0.39, -5.53, 8.73, 10.21], respectively. The developed vector-IM based fragility model could hopefully serve as a tool for assessing the seismic risk of earth slopes in engineering practice.

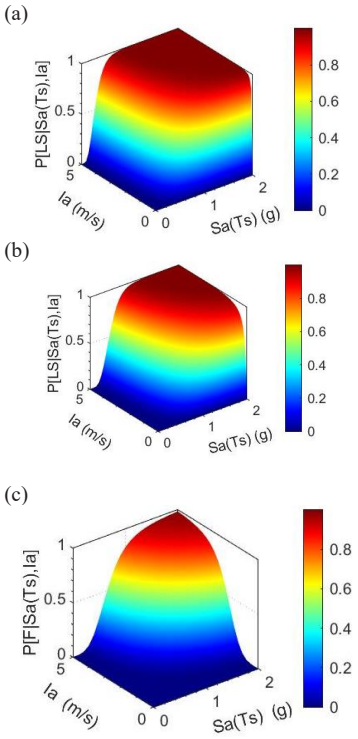

Figure 6. Fragility surfaces of (a) minor damage, (b) moderate damage, and (c) complete failure for man-made earth slope based on [Sa(Ts), Ia], respectively.

6 ACKNOWLEDGEMENTS

The work described was supported by the National Natural Science Foundation of China (Grant No. 51909193).

7 REFERENCES

Ancheta T.D., Darragh R.B., Stewart J.P., and et al. 2014. NGA-West2 database. *Earthq Spectra* 30(3), 989-1005.

Argyroudis S.A. and Kaynia A.M. 2015. Analytical seismic fragility functions for highway and railway embankments and cuts. *Earthquake Engineering and Structural Dynamics* 44(11), 1863-1879.

Argyroudis S.A., Mitoulis S.A., Winter M.G., et al. 2019. Fragility of transport assets exposed to multiple hazards: State-of-the-art review toward infrastructural resilience. *Reliability Engineering & System Safety* 191, 106567-.

Arias A. 1970. A measure of earthquake intensity. Seismic design for nuclear power plants. Cambridge, UK: MIT Press.

Baker J. 2005. Vector-valued ground motion intensity measures for probabilistic seismic demand analysis. Stanford: Stanford University.

Baker J. and Cornell C. 2008. Vector-valued intensity measures incorporating spectral shape for prediction of structural response. *J Earthquake Eng* 12,534-54.

Baker J. 2015. Efficient analytical fragility function fitting using dynamic structural analysis. *Earthquake Spectra* 31(1), 579-599.

Bradley B. 2011. Empirical equations for the prediction of displacement spectrum intensity and its correlation with other intensity measures. *Soil Dyn Earthquake Eng* 31, 1182-91.

Bray J. and Travasarou T. 2007. Simplified procedure for estimating earthquake-induced deviatoric slope displacements. *Journal of Geotechnical and Geoenvironmental Engineering* 133(4), 381-392.

Du W. and Wang G. 2014. Fully probabilistic seismic displacement analysis of spatially distributed slopes using spatially correlated vector intensity measures. *Earthquake Engineering and Structural Dynamics* 43(5), 661-679.

Du W., Wang G., and Huang D. 2018. Evaluation of seismic slope displacement based on fully coupled sliding mass analysis and NGA-West2 database. *Journal of Geotechnical & Geoenvironmental Engineering* 144(8), 06018006.1-06018006.7.

Du W., Yu X., and Ning C.L. 2020. Influence of earthquake duration on structural collapse assessment using hazard-consistent ground motions for shallow crustal earthquakes. *Bulletin of Earthquake Engineering*, 1-19.

EPRI-NP-5930. 1988. A criterion for determining exceedance of the operating basis earthquake, Tech. rep. Palo Alto, CA: Electrical Power Research Institute (EPRI).

Gehl, P., Seyedi D.M., and Douglas J. 2013. Vector-valued fragility functions for seismic risk evaluation. *Bull. Earthquake Eng.* 11 (2), 365-384.

Hao M., Xie L., Xu L. 2005. Some considerations on the physical measure of seismic intensity. *Acta Seismol Sin* 27, 230-234.

Hardin B.O. and Drnevich V.P. 1972a. Shear modulus and damping in soils: measurement and parameter effects. *Journal of the Soil Mechanics and Foundations Division ASCE.* 98(SM6), 603-24.

Hardin B.O. and Drnevich V.P. 1972b. Shear modulus and damping in soils: design equations and curves. *Journal of the Soil Mechanics and Foundations Division ASCE.* 98(SM7), 667-92.

Hariri-Ardebili M.A., Saouma V.E. 2016. Probabilistic seismic demand model and optimal intensity measure for concrete dams. *Structural Safety* 59, 67-85.

HAZUS-MH: User's Manual and Technical Manuals. National Institute of Building Sciences. 2004. Report prepared for the Federal Emergency Management Agency, Washington, D.C. USA.

Hu H., Huang Y., Chen Z. 2019. Seismic fragility functions for slope stability analysis with multiple vulnerability states. *Environmental Geology* 78(24), 690.1-690.10.

Huang H.W., Wen S.C., Zhang J., et al. 2018. Reliability analysis of slope stability under seismic condition during a given exposure time. *Landslides* 15(11), 2303-2313.

Itasca Consulting Group Inc. 2016. FLAC-Fast Lagrangian analysis of continua. Version 8.0. User's Manual.

Jafarian Y., Miraei M. 2019. Scalar- and vector-valued fragility analyses of gravity quay wall on liquefiable soil: example of Kobe port. *International journal of geomechanics* 19(5), 04019029.1-04019029.21.

Jalayer F. 2003. Direct probabilistic seismic analysis: implementing non-linear dynamic assessments. Stanford: Stanford University.

Jalayer F. and Cornell C.A. 2009. Alternative non-linear demand estimation methods for probability-based seismic assessments. *Earthq Eng Struct Dyn.* 38(8), 951-972.

Jalayer F., Beck J., and Zareian F. 2012. Analyzing the sufficiency of alternative scalar and vector intensity measures of ground shaking based on information theory. *J. Eng. Mech.* 138 (3), 307–316.

Jalayer F., Ebrahimian H., Miano A., and et al. 2017. Analytical fragility assessment using unscaled ground motion records. *Earthquake Engineering & Structural Dynamics* 46(15), 2639-2663.

Jin C., Chi S. 2019. Seismic fragility analysis of high earth-rockfill dams considering the number of ground motion records. *Mathematical Problems in Engineering* (PT.4), 6958643.1-6958643.12.

Lagaros N.D., Tsompanakis Y., Psarropoulos P.N., Georgopoulos E.C. 2009. Computationally efficient seismic fragility analysis of geostructures. *Computers and Structures* 87(19-20), 1195-1203.

Luco N. 2002. Probabilistic seismic demand analysis, smrf connection fractures, and near-source effects. Stanford: Stanford University.

Luco N. and Cornell A.C. 2007. Structure-specific scalar intensity measures for near-source and ordinary earthquake ground motions. *Earthquake Spectra* 23, 357-392.

Maruyama Y., Yamazaki F., Mizuno K., et al. 2010. Fragility curves for expressway embankments based on damage datasets after recent earthquakes in Japan. *Soil Dynamics and Earthquake Engineering* 30(11), 1158-1167.

Padgett J., Nielson B., DesRoches R. 2008. Selection of optimal intensity measures in probabilistic seismic demand models of highway bridge portfolios. *Earthquake Eng Struct Dyn* 37, 711-25.

Pan Y., Agrawal A., Ghosn M., and et al. 2010. Seismic fragility of multispan simply supported steel highway bridges in New York State. II: Fragility analysis, fragility curves, and fragility surfaces. *J.Bridge Eng.* 15 (5), 462-472.

PIANC (Permanent International Association of Navigation Congresses). 2001. Seismic design guidelines for port structures. Brussels, Belgium: PIANC.

Pitilakis K., Crowley E., Kaynia A. (eds). 2014. SYNER-G: typology definition and fragility functions for physical elements at seismic risk. *Geotechnical, Geological and Earthquake Engineering* 27, Springer.

Shome N. 1999. Probabilistic seismic demand analysis of nonlinear structures. Stanford: Stanford University.

Trifunac M.D., Brady A.G. 1975. A study on the duration of strong earthquake ground motion. *Bulletin of the Ssmological Society of America* 65(3), 581-626.

Von T.J., Roehm L., Scott G., and et al. 1988. Earthquake ground motions for design and analysis of dams, in Earthquake Engineering and Soil Dynamics II-recent advances in ground-motion evaluation. *Geotechnical Special Publication* 463-81.

Wang G. and Du W. 2012. Empirical correlations between cumulative absolute velocity and spectral accelerations from NGA ground motion database. *Soil Dyn. Earthquake Eng.* 43 (Dec), 229-236.

Wang W., Li D., Liu Y., et al. 2021. Influence of ground motion duration on the seismic performance of earth slopes based on numerical analysis. *Soil Dynamics and Earthquake Engineering* 143(5), 106595.

Werner S.D., Taylor C.E., Cho S., and et al. 2006. REDARS 2: methodology and software for seismic risk analysis of highway systems. MCEER-06-SP08, University at Buffalo, State University of New York.

Wu, Z.X. 2015. Development of fragility functions for slope instability analysis: Fragility functions for slope instability analysis (Technical Note). *Landslides* 12(1), 165-175.

Yakhchalian M., Nicknam A., and Amiri G.G. 2015. Optimal vector valued intensity measure for seismic collapse assessment of structures. *Earthquake Eng. Eng. Vib*. 14 (1), 37-54.